Modern Management Science & Engineering
ISSN ISSN 2052-2576
Vol. 8, No. 1, 2026
www.scholink.org/ojs/index.php/mmse

Original Paper

Research and Design of Reactor Temperature Control System Based on RBF Neural Network

Wenjie Wang[1], Yanan Meng[1*], & Yingxu Huang[1]

[1] Jilin University of Chemical Technology, Jilin, Jilin, China

[*] Corresponding Author

Received: October 28, 2025 Accepted: January 02, 2025 Online Published: January 30, 2026

doi:10.22158/mmse.v8n1p169 URL: http://dx.doi.org/10.22158/mmse.v8n1p169

Abstract

Aiming at the time-varying, nonlinear and large time-delay problems of chemical reactor temperature control systems, this study focuses on the continuous stirred tank reactor (CSTR) for aniline hydrogenation to cyclohexylamine, and conducted modeling, advanced control algorithm design and simulation verification of the temperature control system. The temperature control mathematical model was established by fitting process data with Aspen software and parameter identification via MATLAB System Identification Toolbox. Cascade control schemes of traditional PID, BP neural network PID and LPSO-RBF-PID were designed, and their control performances were compared through Simulink simulation. Results show that the proposed control scheme has significantly better anti-interference ability than traditional ones, providing an effective technical solution for precise temperature control of industrial reactors.

Keywords

Reactor temperature control, RBF neural network, Cascade control, PID

1 Introduction

The chemical industry plays a pivotal role in national economic development (Gheorghe, Ana, Nicolae, & Stela, 2000), and reactors serve as critical production equipment in traditional chemical manufacturing. Continuous Stirred Tank Reactors (CSTRs) are widely used in industrial processes; however, temperature control during reactions is challenged by nonlinearity and large time delays. Consequently, improving the response speed and accuracy of temperature control systems to enhance production efficiency and economic benefits has become a research focus in the industrial sector. To address nonlinear control issues, this study proposes an improved Particle Swarm Optimization (PSO) algorithm to optimize the parameters of an RBF-PID controller, thereby achieving precise temperature

control of CSTRs. In PSO-based optimization, an inertia weight parameter is introduced to improve optimization convergence speed and solution accuracy. The Radial Basis Function (RBF) neural network, proposed by Moody and Darken (2008) in 1989, is a feedforward neural network capable of approximating any continuous function with arbitrary precision. Since its inception, it has garnered extensive attention and been widely applied to system identification, data prediction, and other fields. For instance, Obaid Alshammari et al. (2021) proposed a neural network-based adaptive backstepping control law for the Continuous Stirred Tank Reactor (CSTR). Shi Li et al. M. Rajendra et al. (2015) proposed a Complex-space Radial Basis Function neural network (CRBF), which is applied to the identification of multiple cracks in cantilever beams in the frequency domain. ALSHAMMARI, MAHYUDDIN, and JERBI (2020) put forward a model predictive control algorithm based on a radial basis function neural network model and applied this algorithm to a nonlinear CSTR process. Shiwei Yu et al. (2019) proposed a hybrid algorithm integrating PSO and genetic algorithms to optimize RBF neural networks, thereby establishing a hybrid model for power demand forecasting. This model uses hybrid-coded particles (binary and real-valued) to optimize the RBF network structure via genetic algorithms and adjust network parameters through the PSO-GA hybrid algorithm. Results indicated that the proposed hybrid model features a simpler structure and higher prediction accuracy.

Nevertheless, RBF neural networks suffer from high computational complexity and difficulties in parameter determination. Conventional training algorithms struggle to find the global optimal values for center vectors and width parameters; moreover, to achieve satisfactory approximation performance, these algorithms often require a large number of hidden layer nodes, leading to increased computational load. Therefore, this study adopts an improved PSO algorithm to optimize key parameters of the RBF controller for parameter identification, verifying its impact on the reactor temperature control system. Targeted adjustments and improvements to the optimization process are made based on actual operating conditions to achieve high-performance control of the controlled plant. Simultaneously, different control systems are established using MATLAB/Simulink to generate response curves. Control indices of the reactor temperature control system under various conditions are compared to validate the advantages of the improved PSO-RBF control algorithm.

2. Aniline Hydrogenation Reactor Control System

This study is based on the aniline hydrogenation process for cyclohexylamine production in an industrial plant, focusing on precise temperature control of the reactor. Cyclohexylamine is a high-value fine chemical product with critical applications across multiple fields: in pharmaceuticals, it serves as a component in antibiotics for disease treatment; in chemistry, it acts as a catalyst—significantly reducing reaction activation energy to facilitate refractory or slow reactions, and accurately guiding reaction directions in organic synthesis to support the development of new substances and process innovation. The CSTR employed in this study is fabricated from corrosion-resistant and high-temperature-resistant 304 stainless steel, featuring a cylindrical shape with

a flat bottom, a diameter of 3 meters, a height of 4.6 meters, and a total volume of 34 m³. To ensure uniform mixing of reactants, a paddle stirrer is installed inside the reactor, with its rotational speed and direction adjustable via an electric motor. The reactor is equipped with an external jacket for heat transfer, and temperature regulation is achieved by adjusting the flow rate of cooling water or steam. An industrial-grade insertion-type Pt100 sensor is selected for temperature measurement, offering high precision and long-distance signal transmission capabilities to meet industrial on-site requirements. Five common production methods for cyclohexylamine exist in industry; this study focuses on the reductive hydrogenation of aniline due to its prominent advantages: (1) a relatively high reaction rate under specific conditions, enabling efficient raw material conversion in a short time; (2) a high recovery rate, ensuring efficient utilization of raw materials to reduce costs, with process optimization achievable through precise control of temperature, pressure, and other parameters to improve product purity and yield; (3) a simplified process flow, eliminating complex intermediate product treatment and tedious process steps compared to multi-step synthesis, thereby reducing operational complexity and time costs for more efficient and controllable production. The complete process flow of aniline hydrogenation to cyclohexylamine is illustrated in Figure 1, depicting the sequence from raw aniline input, through hydrogenation reaction, product separation, and purification, to the final acquisition of high-purity cyclohexylamine and dicyclohexylamine products.

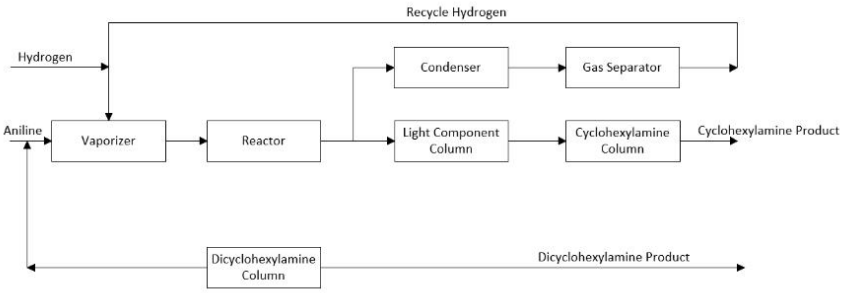

Figure 1. Flow Chart of Cyclohexylamine Process

In the aniline hydrogenation process, temperature is a critical parameter influencing reaction progress: on one hand, moderately increasing the reactor temperature can effectively accelerate the reaction rate, thereby improving production efficiency; on the other hand, excessively high temperatures pose significant risks, including catalyst deactivation and the formation of side reactions. Studies have shown that when the temperature is controlled below 250°C, the reaction stably produces the target product cyclohexylamine; however, exceeding 250°C leads to the generation of by-products such as aniline, which impairs reaction stability and product purity. Therefore, clarifying the quantitative relationship between temperature and reaction rate is essential for achieving precise temperature control, balancing reaction efficiency, and ensuring product quality.

3. Establishment of Reactor Temperature Model

The relationship between chemical reaction rate and temperature in industrial processes is described by the Arrhenius equation, where the reaction rate increases with temperature:

$$k = k_0 \exp(-\frac{E}{RT}) \tag{1}$$

k—Reaction rate constant (L/(mol·h)); k_0—Frequency factor (L/(mol·h)); E—Activation energy (the average energy required for reactant molecules to become active molecules capable of reacting); R—Molar gas constant (R = 1.987 cal/(mol·K)); T—Absolute temperature of the reactor (K).

Heat balance is crucial in the chemical reaction system of a CSTR. Due to the material properties of the reactor and jacket, volume expansion/contraction and density fluctuations are negligible under slight variations in reaction conditions. To simplify model establishment while ensuring accuracy for research and process control, this study assumes constant volume and density for both the reactor and jacket. Based on these assumptions, the heat balance equation of the reactor system under steady-state conditions—representing the sum of heat accumulation inside the reactor and heat loss to the environment—is expressed as:

$$Q = C\frac{dT}{dt} + \frac{T - T_0}{R} \tag{2}$$

Q—Total heat inside the reactor plus heat loss;C—Heat capacity of the reactor;T—Temperature inside the reactor;t—Reaction time;T_0—Ambient temperature;R—Thermal resistance

Taking the Laplace transform of Equation (2) yields:

$$Q(s) = CsT(s) + \frac{T(s)}{R} \tag{3}$$

In practical operation, the reactor exhibits thermal inertia—temperature does not respond immediately to heating or cooling, but gradually approaches the target temperature after a delay. Additionally, the response time of measuring elements and environmental interactions cause delays in signal transmission, resulting in a time lag between measured values and actual temperatures. Therefore, a delay link is introduced between the control signal and the temperature transmitter output:

$$G(s) = \frac{kT(s)}{Q(s)} = \frac{k}{Cs + R}e^{-\tau s} = \frac{K}{Ts + 1}e^{-\tau s} \tag{4}$$

k—Proportional signal；T=RC—Time constant；K=kR—Process gain； τ —Time delay.

The heat balance equation for the reactor interior is:

$$MC_p\frac{dT}{dt} = V_R(-\Delta H)r(C_A, T) + UA_R(T_C - T) \tag{5}$$

The heat balance equation for the jacket is:

$$V_C\rho_C C_{pC}\frac{dT_C}{dt} = W\rho_C C_{pC}(T_H - T_C) + UA_R(T - T_C) \tag{6}$$

The chemical reaction rate is:

$$r(C_A,T) = kC_A = k_0 \exp(-\frac{E}{RT})C_A \tag{7}$$

Cp—Specific heat capacity of reactants in the reactor; CA—Concentration of reactants in the reactor; M—Total mass of reactants; VR—Volume of reactants; U—Overall heat transfer coefficient of the reactor wall; AR—Heat transfer area of the reactor wall; TC—Coolant outlet temperature; △H—Molar reaction enthalpy; VC—Volume of coolant in the jacket; ρC—Density of coolant in the jacket; CpC—Specific heat capacity of coolant in the jacket; W—Coolant flow rate; TH—Coolant inlet temperature. After Laplace transform and rearrangement, the transfer function of coolant flow rate to reactor temperature is derived as:

$$G(s) = \frac{T(s)}{W(s)} = \frac{a_{12}b_{22}}{s^2 - (a_{11} + a_{22})s + (a_{11}a_{22} - a_{12}a_{21})} \tag{8}$$

Open-loop controllers designed based on the above relationships can only achieve stable temperature control under ideal conditions. However, deviations between the set temperature and actual operating temperature exist in practical industrial scenarios, making pure open-loop control inadequate for process requirements. To address this, a closed-loop control system is constructed: the system takes the deviation between the set temperature and actual reactor temperature as the input variable, and the opening of the cooling water control valve as the core control variable. By dynamically adjusting the valve opening, the coolant flow rate is modified to regulate the reactor temperature. The adjusted temperature is then fed back to the input terminal, forming a complete closed-loop feedback loop to effectively offset temperature deviations and achieve dynamic stable control of the reactor temperature. Considering the need for simplified industrial modeling while ensuring the accuracy of dynamic process characteristics, the mathematical model can be approximated as a first-order inertial delay element:

$$G(s) = \frac{K}{Ts+1}e^{-\tau s} \tag{9}$$

Temperature control of irreversible exothermic reactions is the most challenging in reactor operation; thus, this study focuses on the irreversible exothermic reaction of aniline hydrogenation to cyclohexylamine. Cooling water at 20°C was selected medium. The reactor temperature control structure was built in Aspen Plus, as shown in Figure 2.

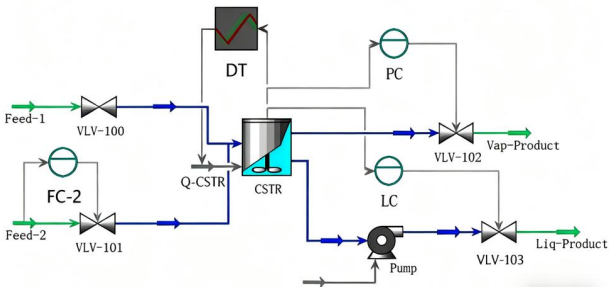

Figure 2. CSTR Control System Flow Chart

Forty-eight sets of measured reactor temperature data from a CSTR in a chemical company were used in this study. The temperature variation trend, as depicted in Figure 3, shows stable operation around 120°C.

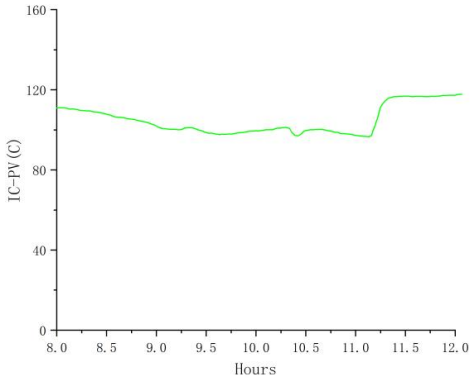

Figure 3. Historical Temperature Measurement Data of the Reactor

The MATLAB System Identification Toolbox was employed for model parameter fitting. Given the reactor's thermal inertia, sufficient data are required to reflect dynamic temperature changes; thus, a sampling time of 2 seconds was selected in MATLAB to effectively capture the relationship between heating factors and temperature variations. Based on the reactor heating model, a first-order inertia delay link was chosen from the Process Models library. After data preprocessing and multiple experiments, the fitting model with the highest matching degree to the actual data was obtained. The final transfer function for reactor temperature control is:

$$G_2(s) = \frac{3}{75s+1} e^{-20s} \tag{10}$$

The transfer function of the control valve, derived using the same method, is as follows:

$$G(s) = \frac{3}{s^2 + 56s + 1} \tag{11}$$

4. Particle Swarm Optimization Algorithm and Improvement Based on RBF-PID

The RBF neural network is a locally responsive feedforward neural network emerging in the late 1980s, rooted in radial basis function interpolation. It consists of an input layer, a radial basis hidden layer, and an output layer. Compared to globally approximating BP neural networks, RBF networks avoid local minimum issues but have higher requirements for sample data. Their hidden layer centers and widths can be determined via K-means clustering, and output weights are solved using the linear least squares method, resulting in faster response speeds. Additionally, the hidden and output layers can be optimized independently, featuring a simple structure. In reactor temperature control, real-time response to local temperature fluctuations is essential. The Gaussian function, with its exponential decay characteristic,

is sensitive only to inputs near its center—enabling rapid focus on temperature changes in critical regions, suppressing noise far from the center, and enhancing system robustness. Thus, it is selected as the basis function for the RBF neural network's hidden layer:

$$\phi_j(\mathbf{x})=\exp\left(-\frac{d_j^2}{2\sigma_j^2}\right) \mathrm{j}=1,2,3,\cdots,\mathrm{j} \tag{12}$$

$$\boldsymbol{x}=[x_1,x_2,\ldots,x_n]^T \tag{13}$$

$$\boldsymbol{c}_j=\left[c_{j1},c_{j2},\ldots,c_{jn}\right]^T \tag{14}$$

J—Number of neurons in the radial basis hidden layer; **x** —n-dimensional input vector;$\mathbf{c}_j$—n-dimensional center vector (same dimension as x);b=(b_1,b_1,⋯,b_j)—spread vector; Squared Euclidean distance between the input vector x and center vector cj , calculated as:

$$d_j^2=\sum_{i=1}^{n}\left(x_i-c_{ji}\right)^2 \tag{15}$$

The key to RBF neural network application lies in determining three parameters: the center vector $\boldsymbol{c}_j$, spread vector $\boldsymbol{b}_j$, and output weights $\boldsymbol{\omega}_j$. The hidden layer maps input data to a high-dimensional space via radial basis functions, which are then linearly combined with the output layer—enabling high-precision approximation of complex nonlinear functions with a small number of hidden nodes. Conventional algorithms typically use K-means clustering on historical temperature data to initialize and $\boldsymbol{b}_j$, and solve via the linear least squares method. However, improper selection of center vectors can lead to slow response speeds, poor accuracy, and only local optimal solutions, failing to achieve ideal control performance. Therefore, the PSO algorithm is proposed to optimize the key parameters of the RBF controller Figure 4, aiming to minimize overshoot and settling time while shortening rise time in the reactor control scheme.

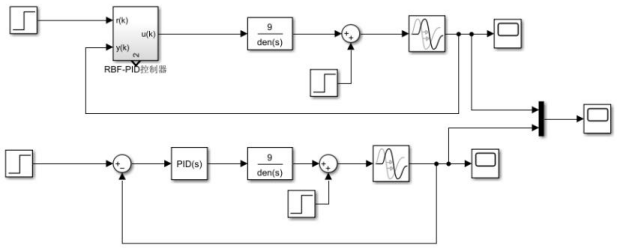

Figure 4. Simulation Structure Diagram of RBF-PID

5. Improved PSO for RBF Neural Network Optimization

The Particle Swarm Optimization (PSO) algorithm, proposed by Kennedy and Eberhart in 1995, is a swarm intelligence global optimization algorithm inspired by collective behaviors such as bird flocking for foraging. Featuring few parameters, easy implementation, and both global exploration and local exploitation capabilities, it is suitable for continuous optimization problems but faces the risk of falling into local optima. By balancing search directions through inertia weight and enhancing diversity via random factors, PSO is widely applied in engineering optimization, machine learning, and other fields.

Its core lies in information sharing and collaboration among particles: by tracking the historical optimal positions of individuals and the swarm, combining inertial, individual cognitive, and social cognitive components to update velocities and positions, particles gradually approach the global optimal solution.In the algorithm, each particle moves in the solution space, adjusting its position based on personal and collective experience. Let denote the historical optimal position of particle i (pbest), and$\mathbf{G}_j=\left(G_1,G_2,\cdots,G_J\right)$ denote the global optimal position of the entire swarm (gbest). Let represent the current position of particle i, and represent its current velocity. Particles update their velocity and position in each iteration using the following equations:

$$v_i(t+1)=w\cdot v_i(t)+c_1r_1\cdot\left(pbest_i-x_i(t)\right)+c_2r_2\cdot\left(gbest-x_i(t)\right) \tag{16}$$

$$x_i(t+1)=x_i(t)+v_i(t+1) \tag{17}$$

$v_i(t)$—Velocity of particle i at time t; $x_i(t)$—Position of particle i at time t; ω—Inertia weight; c_1, c_2—Individual and social learning factors, respectively (typically set to c1=c2 within the range of 0–2); r_1, r_2—Random numbers uniformly distributed in [0,1], introduced to enhance exploration randomness.

To ensure algorithm reliability, constraints are imposed on both particle velocity vi(t) and position xi(t):Velocity limiting: Excessively high particle velocities can degrade convergence. Thus, a maximum velocity threshold is typically set: $v_i(t+1)=\text{sign}\left(v_i(t+1)\right)\cdot\min(|v_i(t+1)|,v_{max})$ If v_{max} is not specified, the inertia weight ω is usually set to less than 1 to naturally limit velocity growth. Boundary handling: To prevent particles from exceeding the solution space, three methods are commonly used: Clamping, Reflection, and Random Reinitialization. This study adopts the Clamping method, as PID parameter optimization for reactors typically has clear physical ranges. Combined with reasonable parameter ranges, velocity limits, and fitness function design, this ensures efficient convergence of the algorithm to a PID parameter combination that meets control performance requirements. To address the limitations of traditional PSO (e.g., local optima trapping and insufficient global search capability), an improved PSO (LPSO) is proposed Figure 5, integrating Logistic chaotic initialization and Levy flight strategies:

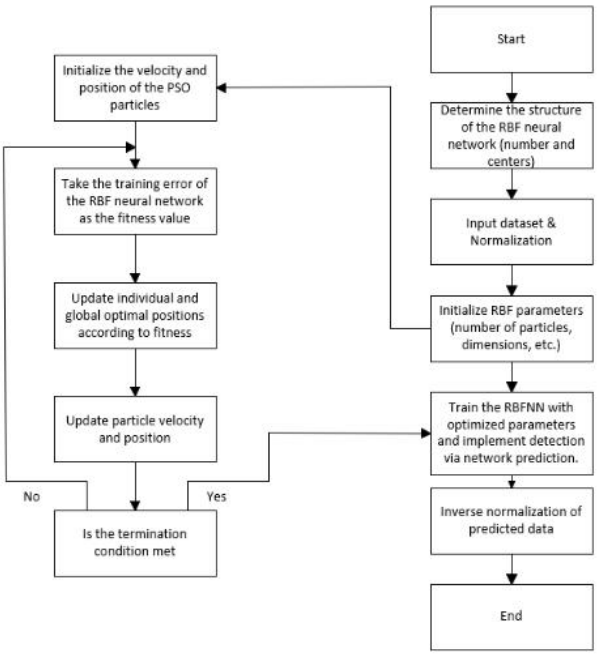

Figure 5. LPSO-RBF Flow Chart of the Hybrid Model

6. Comparison of Simulation Results

Figure 6 and Figure 7 presents the response curves of the LPSO-RBF-PID control system and the system response curves with a 5-unit disturbance introduced at 600s. Traditional PSO relies solely on the classic velocity update formula consisting of three components—inertial term, individual cognitive term, and social cognitive term—as follows: $\omega=\exp\left(\frac{m}{c_{max}^2}\ //\ X\text{-}C_j\ //^2\right)$, $j=1,2,\ldots,m$. In contrast, LPSO demonstrates distinct advantages over conventional PSO: conventional PSO is prone to falling into local optima and lacks sufficient global search capability, while the improved PSO (LPSO) expands the global search range through chaotic initialization and retains local exploitation ability via Levy flight, achieving a balance between the two. PID controllers optimized by conventional PSO exhibit large overshoot, slow adjustment, and high steady-state error in complex

systems, whereas those optimized by LPSO feature small overshoot, fast adjustment, and low steady-state error.

LPSO integrates chaotic functions with Levy random search strategies. Specifically, the Logistic chaotic map is adopted to optimize the initial distribution of particles, ensuring that RBF parameters and PID parameters (Kp, Ki, Kd) are more uniformly distributed in the solution space. This enables precise matching with the control requirements of the aniline hydrogenation to cyclohexylamine reactor—after optimization, the system can real-time identify fluctuations in reactor operating conditions, maintain temperature stability, and avoid declines in reaction efficiency. For the Levy flight procedure, the beta step size is set to 1.5 and the compensation coefficient to 0.01, tailored to the

temperature delay and complexity of the reactor. Compared to conventional PSO, LPSO balances global search and local development capabilities, making it more suitable for high-dimensional, multi-modal complex problems.

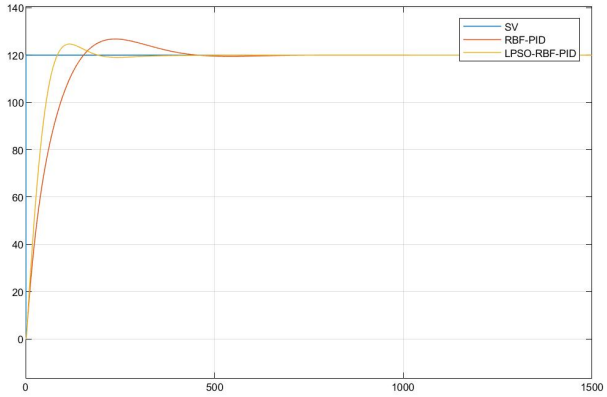

Figure 6. LPSO-RBF-PID Control System Response Curves

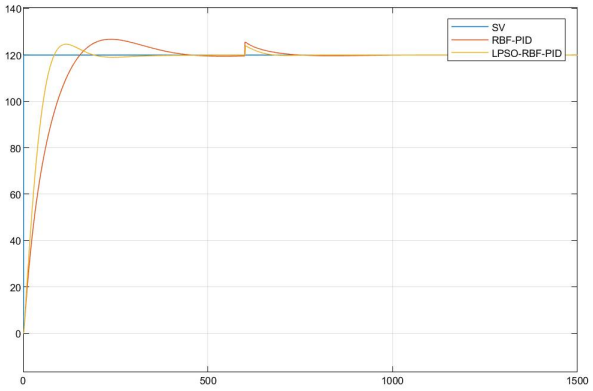

Figure 7. LPSO-RBF-PID Anti-Interference Test Simulation Curve

Experimental results are illustrated in the figures:

(1) The curve tuned by the RBF-PID controller exhibits an overshoot of approximately 0.085, a settling time of about 650s, and a rise time of around 150s;

(2) The curve optimized by the LPSO-RBF-PID algorithm achieves an overshoot of approximately 0.042, a settling time of about 375s, and a rise time of around 100s;

(3) The LPSO-RBF-PID-optimized curve demonstrates excellent tracking performance, anti-interference ability, and robustness, with ideal simulation results.

7. Conclusion

As observed from the anti-interference test simulation curves, when a 5-unit disturbance is introduced at 600s, the response curve optimized by LPSO only exhibits a dynamic deviation of 2%, indicating

markedly improved anti-interference performance. This verifies the effectiveness of the cascade control structure in improving the anti-interference performance of the reactor constant temperature system.

References

ALSHAMMARI, O., MAHYUDDIN, M. N., & JERBI, H. (2020). A neural network-based adaptive backstepping control law with covariance resetting for asymptotic output tracking of a CSTR plant. *IEEE Access*, *8*, 29755-29766. https://doi.org/10.1109/ACCESS.2020.2972621

Gheorghe, N., Ana, O., Nicolae, A., & Stela, D. (2000). Thermal Effectsof Some Polymerization and Polycondensation Reactions. Polymeric Quaternary Salts. *European Polymer Journal*, 2679-2680. https://doi.org/10.1016/S0014-3057(00)00053-7

LI, S., JIANG, P., & HAN, K. (2019). Rbf neural network based model predictive control algorithm and its application to a cstr process; proceedings of the 2019 Chinese control conference (CCC), F, 2019 [C]. *IEEE*. https://doi.org/10.23919/ChiCC.2019.8865797

Moody, J., & Darken, C. J. (2000). Fast Learning in Networks of Locally-Tuned Processing Units. *Neural Computation*, *1*(2), 281-294. https://doi.org/10.1162/neco.1989.1.2.281

PANG, F., LUO, M., XU, X. et al. (2021). Path Tracking Control of an Omni-Directional Service Robot Based on Model Predictive Control of Adaptive Neural-Fuzzy Inference System. *Applied Sciences*, *11*(2), 838. https://doi.org/10.3390/app11020838

Rajendra, M., & Shankar, K. (2015). Improved Complex-valued Radial Basis Function(ICRBF)neural networks on multiple crack identification. *Applied Soft Computing*, *28*(C), 285-300. https://doi.org/10.1016/j.asoc.2014.10.044